Received: 17 July 2017 | Accepted: 2 November 2017
DOI: 10.1002/hyp.11399

WILEY

RESEARCH ARTICLE

Infiltration into frozen soil: From core-scale dynamics to hillslope-scale connectivity

Willemijn M. Appels | **Anna E. Coles** | **Jeffrey J. McDonnell**

Global Institute for Water Security & School of Environment and Sustainability, University of Saskatchewan, 11 Innovation Boulevard, Saskatoon, SK S7N 3H5, Canada

Correspondence
Willemijn M. Appels, Lethbridge College, 3000 College Drive S, Lethbridge, AB T1K 1L6, Canada.
Email: willemijn.appels@gmail.com

Present Address
A. E. Coles, Wilfrid Laurier University, 5007 50 Avenue, Yellowknife, NT X1A 2P8, Canada.

Abstract

Infiltration into frozen soil is a key hydrological process in cold regions. Although the mechanisms behind point-scale infiltration into frozen soil are relatively well understood, questions remain about upscaling point-scale results to estimate hillslope-scale run-off generation. Here, we tackle this question by combining laboratory, field, and modelling experiments. Six large (0.30-m diameter by 0.35-m deep) soil cores were extracted from an experimental hillslope on the Canadian Prairies. In the laboratory, we measured run-off and infiltration rates of the cores for two antecedent moisture conditions under snowmelt rates and diurnal freeze–thaw conditions observed on the same hillslope. We combined the infiltration data with spatially variable data from the hillslope, to parameterise a surface run-off redistribution model. We used the model to determine how spatial patterns of soil water content, snowpack water equivalent (SWE), and snowmelt rates affect the spatial variability of infiltration and hydrological connectivity over frozen soil. Our experiments showed that antecedent moisture conditions of the frozen soil affected infiltration rates by limiting the initial soil storage capacity and infiltration front penetration depth. However, shallow depths of infiltration and refreezing created saturated conditions at the surface for dry and wet antecedent conditions, resulting in similar final infiltration rates (0.3 mm hr^{-1}). On the hillslope-scale, the spatial variability of snowmelt rates controlled the development of hydrological connectivity during the 2014 spring melt, whereas SWE and antecedent soil moisture were unimportant. Geostatistical analysis showed that this was because SWE variability and antecedent moisture variability occurred at distances shorter than that of topographic variability, whereas melt variability occurred at distances longer than that of topographic variability. The importance of spatial controls will shift for differing locations and winter conditions. Overall, our results suggest that run-off connectivity is determined by (a) a pre-fill phase, during which a thin surface soil layer wets up, refreezes, and saturates, before infiltration excess run-off is generated and (b) a subsequent fill-and-spill phase on the surface that drives hillslope-scale run-off.

KEYWORDS
hydrological connectivity, infiltration into frozen ground, spatial variability of snowpack, spring snowmelt

1 | INTRODUCTION

Infiltration into frozen soil is an important hydrological flux in cold regions (Fang & Pomeroy, 2007; Ireson, van der Kamp, Ferguson, Nachson, & Wheater, 2013). In these regions, spring snowmelt is typically the dominant hydrological event of the year. On the Canadian Prairies, where frozen ground persists through the melt season, snowmelt drives up to 80% of annual run-off. The partitioning of snowmelt between infiltration into frozen soils and run-off determines flooding (Gray, Landine, & Granger, 1985; Kane & Stein, 1984; Li & Simonovic, 2002), soil moisture variability and availability for crop production (Gray, Norum, & Granger, 1984; McConkey, Ulrich, & Dyck, 1997), and solute transport (Su et al., 2011). Understanding infiltration into frozen soil is therefore crucial for predicting these water resource issues.

Gravity and capillary forces drive infiltration into frozen soil. Capillary processes are more complex in frozen than in unfrozen soils due to coupled energy and mass transfer associated with phase changes

(Kane & Stein, 1983). A frozen soil is a continuum of particles: large air-filled pores, intermediate ice-filled pores, small liquid water-filled pores, and liquid water films around particles (Stähli, Jansson, & Lundin, 1999). The extent to which pores are filled with air, ice, and water are determined by soil water content before freeze-up and pore size distribution (Watanabe & Wake, 2009). Ice-filled pores decrease the total pore space and increase the tortuosity of the remaining pore space, resulting in a lower hydraulic conductivity of the remaining pore domain and consequently reduced infiltration rates compared to unfrozen soils (Stähli et al., 1999). The soil water content before freeze-up is therefore a key variable in empirical frozen soil infiltration equations (Granger, Gray, & Dyck, 1984; Zhao & Gray, 1997). Heat transport affects infiltration rates into frozen soils more than those into unfrozen soils. When soils remain frozen during the melt period, infiltrated water refreezes in the infiltration zone, limiting rates even further (Stähli et al., 1999), whereas soil thaw during the infiltration period is accompanied by sudden jumps in infiltration rates (Hayashi, van der Kamp, & Schmidt, 2003; Watanabe et al., 2012).

Despite having identified most of the physical aspects of the infiltration into frozen soil process —amassed from a plethora of laboratory (e.g., Lilbæk & Pomeroy, 2010; McCauley, White, Lilly, & Nyman, 2002; Watanabe et al., 2012), field (e.g., Bayard, Stähli, Parriaux, & Flühler, 2005; Granger et al., 1984; Hayashi et al., 2003; Iwata, Hayashi, Suzuki, Hirota, & Hasegawa, 2010; Kane & Stein, 1983, 1984), and modelling studies (e.g., Gray et al., 1985; Gray, Toth, Zhao, Pomeroy, & Granger, 2001; Hansson, Šimůnek, Mizoguchi, Lundin, & van Genuchten, 2004; Jansson & Karlberg, 2001; Kane, Hinkel, Goering, Hinzman, & Outcalt, 2001; Kitterød, 2008; Ling & Zhang, 2004; Motovilov, 1978, 1979; Painter, 2011; Romanovsky & Osterkamp, 2000; Zhao & Gray, 1997; Zhao, Gray, & Male, 1997)—we still struggle to apply our point-scale understanding to the hillslope- and catchment-scales. This has implications for our ability to predict run-off generation, soil moisture conditions, and solute transport occurring at those larger scales.

The scaling difficulties lie partly in the presence of environmental factors, for example, wind-driven snow redistribution, land-use-driven accumulation, and soil insulation, which may affect melt, thaw, and thereby the infiltration process itself (Hayashi, 2013). They can also be attributed to the design of laboratory studies, in which the use of repacked (as opposed to intact) soil columns and a focus on ponded water conditions are typical (Hansson et al., 2004; Lilbæk & Pomeroy, 2010; McCauley et al., 2002; Moghadas, Gustafsson, Viklander, Marsalek, & Viklander, 2016; Watanabe et al., 2012). With the notable exception of the study of Watanabe and Kugisaki (2017), who conducted one-dimensional column experiments with macroporous soils, these typical laboratory studies cannot be easily scaled to understand field conditions where macropore flow and nonponded infiltration may dominate (Ishikawa, Zhang, Kadota, & Ohata, 2006; Stähli, Jansson, & Lundin, 1996). But infiltration into frozen soil is also very difficult to measure directly in the field (Baker, 2006) because of instrument error in sub-zero conditions and the effects of an overlying snowpack. As a result, in the field, hillslope-averaged melt into frozen soil is usually deduced from snowpack and run-off observations, which unfortunately reveal little about the spatial variability in infiltration or soil water content. Finally, a paucity of reliable data and the complexities associated with solving the coupled energy and water balance mean infiltration into frozen soil is notoriously difficult to validate with hydrological models (Gupta & Sorooshian, 1997; Pomeroy et al., 2007).

So what can be done? It is imperative that we bridge the gap between core-scale and hillslope-scale understanding of infiltration into frozen soil. Here, we tackle this research challenge with a combined laboratory, field, and modelling experiment. We undertook laboratory experiments on large, intact soil cores extracted from a 5 ha experimental hillslope on the Canadian Prairies. The laboratory experiments simulated nonponding snowmelt conditions during a multiday event, where the soil water content, air temperature and snowmelt rates were driven with observed data from a field season in spring 2014 at the same 5 ha experimental hillslope (Coles & McDonnell, 2017). We then combined the laboratory-generated, core-scale infiltration data, with spatially variable hillslope-scale data observed during the 2014 field season, to parameterise a surface run-off redistribution model. We used that model to determine how the spatial patterns of the hydrological variables relevant during spring melt affects the spatial variability of infiltration into frozen soil and run-off generation at the hillslope-scale.

Overall, our novel core- to hillslope-scales study of infiltration into frozen soil sought to answer the following questions:

1. What is the relationship between soil water content at freeze-up and core-scale infiltration and run-off rates during snowmelt?
2. How does this relationship affect the spatial variability of infiltration-run-off partitioning at the hillslope-scale?
3. To what extent does the spatial variability of hydrological variables (soil water content at freeze-up, snowpack snow water equivalent [SWE], and snowmelt rate) influence hillslope-scale infiltration-run-off patterns?

2 | METHODS

2.1 | Soil core extraction and instrumentation

We extracted six undisturbed soil cores from a hillslope at the Swift Current Research and Development Centre in Swift Current (SK, Canada) in June 2014. This is one of three experimental hillslopes in the 1962–2013 run-off, precipitation, and soil water content monitoring programme of Agriculture and Agri-Food Canada (Coles, McConkey, & McDonnell, 2017) and the location of the hillslope-scale observations described below (Coles & McDonnell, 2017). We constructed a stainless steel corer to extract six 0.30 m in diameter by 0.35 m high intact soil cores. The corer approach followed Tindall, Hemmen, and Dowd (1992) with a vertical disarticulating spring-apart seam to enable the soil core to be removed intact from the corer. We used a hydraulic press to push the corer into the ground and then used hand shovels to carefully excavate the earth from around the outsides of the buried corer, and lift it from the ground. We removed the stainless-steel corer and wrapped the soil core in flexible sheet metal (5×10^{-4} m thick, 0.40 m high, and 1.05 m wide) to form a cylinder 0.40 m high around the soil core. The top of the cylinder was 0.05 m above the surface of the soil core. The base of the soil core was loosely wrapped in a coarse mesh fabric that allowed water to freely drain from the bottom of the core but prevented chunks of soil from breaking off the cores. The sheet metal and mesh fabric were held in place with hose clamps.

We drilled through the metal casing at pre-determined depths in order to instrument the soil cores to monitor soil water content and temperature. The soil cores were instrumented with four Stevens HydraProbe II soil water content sensors at depths of: 0.05 m (2), 0.15 m (1), and 0.25 m (1) for volumetric water content—θ_{TOP}, θ_{MID}, and θ_{BASE}, respectively (Figure 1). We also installed 19 thermocouples (Type T Copper/Constantan) at increments of 0.01 m over depths of 0.01–0.10 m and increments of 0.02 m over depths of 0.12–0.28 m, to measure temperature through the soil core (Figure 1). Soil water content and temperature data were logged at 30-s intervals.

The cores were wrapped in insulating material, maintaining frozen conditions in the body of the cores, as the air temperature of the freezer was increased. The top and bottom of the cores were directly exposed to the air temperature of the freezer. The tops were more exposed to airflow than the bottom, due to the very small space between the bottom of the cores and the lab bench on which they were placed. Upward soil thaw at the bottoms of the cores could occur, especially at low initial moisture content. At the beginning of the experiment, we anticipated that the penetration of such a thaw front would not be large enough to affect the infiltration front. This assumption was checked with temperature data from lower depths in the cores.

2.2 | Core-scale simulated snowmelt events

We conducted two simulated snowmelt event experiments, with three replicate cores for each event. The experiments were differentiated by their antecedent soil moisture conditions: dry (0.11 $m^3\ m^{-3}$) and wet (0.18 $m^3\ m^{-3}$). We dried down or wetted up the cores to the desired start conditions, after which we froze the cores in a walk-in freezer. We sloped the surface of the soil cores at an angle of 5% to collect surface run-off. Each experiment was 4 days in duration with diurnal freezing and thawing, where we varied the air temperature of the freezer between −5 and +2°C according to measured diurnal temperature conditions in the field. We applied 50 mm of "snowmelt" water directly to the surface of the soil cores using a plant sprayer, with rates varying between 0 and 160 mm d^{-1}. This represented snowmelt rates observed during the main melt period of the 2014 snowmelt season at the Swift Current site as described by Coles and McDonnell (2017). The air temperature fluctuations and snowmelt applications were carried out in real time (i.e., 1 hr of experiment = 1 hr of observed data from the field). The temperature of the "snowmelt" water was maintained at 0–1 °C by keeping ice in the water buckets. We added brilliant blue dye to the "snowmelt" water applied to one core in the dry experiment. After that experiment, we dissected the dyed core by cutting vertical and horizontal sections for qualitative analysis of infiltration patterns and any preferential flow pathways, following methods of Flury, Flühler, Jury, and Leuenberger (1994) and Weiler and Flühler (2004).

Any surface run-off during the experiments was routed through a hole in the core's metal casing at the downslope end of the core and collected in a small bucket. We recorded run-off volumes (mL) on an hourly basis and converted these to run-off rates (mm hr^{-1}). We used the snowmelt and run-off rates to determine infiltration rates and infiltration capacities of the soil. Instead of using a dedicated infiltration equation for frozen soils, we used the format of Philip's infiltration equation originally derived for unfrozen soils (Philip, 1957a). The following equation was fitted to the observed time series of infiltration rate on the days that run-off was generated:

$$I_C = \frac{S_a}{2\sqrt{t}} + K_e, \tag{1}$$

where I_C is infiltration capacity (m d^{-1}), S_a is the apparent sorptivity (m $d^{-1/2}$), t is time (d), and K_e is the final infiltration capacity or effective saturated hydraulic conductivity of the frozen soil (m d^{-1}). In the original Philip infiltration equation, sorptivity is a measure of the ability of soil to absorb liquid by capillarity, affected by soil texture and initial

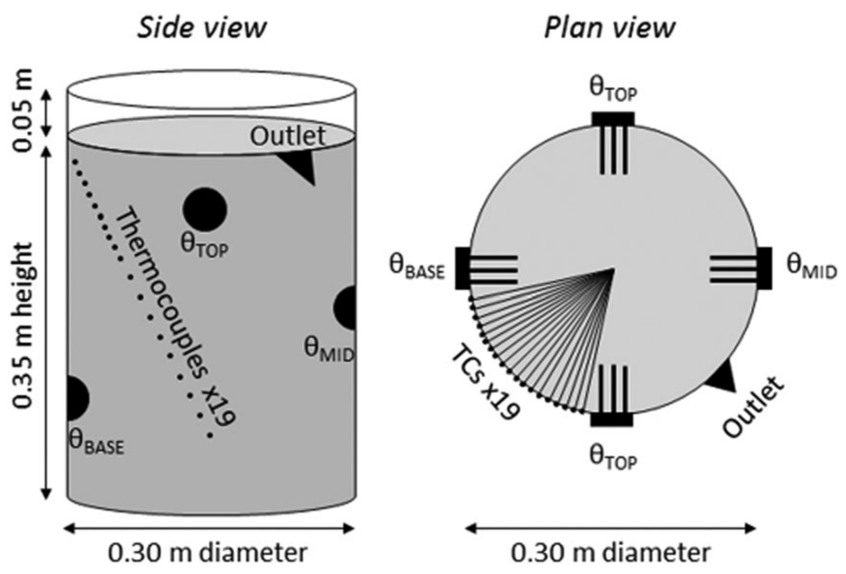

FIGURE 1 Dimensions and instrumentation of the experimental soil cores in side view and plan view

moisture content of the soil (Philip, 1957b). In our adoption of the equation for frozen soils, S_a is not a measure of a physical property but a proxy for the tortuosity increase due to ice-filled pores. Fitting Equation 1 to the data resulted in an estimate of S_a as a function of combined ice and liquid water content (θ_{TOT}) in the upper 0.10 m of the cores and an estimate of K_e.

Further, data from the Stevens HydraProbe II soil water content sensors and thermocouples were used to infer the position of the infiltration front over time. Various correction and calibration procedures have been proposed to measure liquid water content in frozen soils with standard dielectric soil water content sensors (Birchak, Gardner, Hipp, & Victor, 1974; Roth, Schulin, Flühler, & Attinger, 1990; Seyfried & Murdock, 1996; Spaans & Baker, 1995; Watanabe & Wake, 2009). We applied a dielectric mixing model (Birchak et al., 1974) to incorporate the effect of low permittivity of absorbed water and the permittivity of ice. In this model, liquid water content in unfrozen (θ when $T \geq 0$) and frozen soils (θ_u when $T < 0$) are calculated with

$$\begin{aligned} \theta\left(\varepsilon_{bw}^{\alpha}-\varepsilon_{a}^{\alpha}\right) &= \left(\varepsilon_{r}^{\alpha}-\varepsilon_{a}^{\alpha}\right)-\theta_s\left(\varepsilon_{s}^{\alpha}-\varepsilon_{a}^{\alpha}\right) && (T\geq 0), \\ \theta_u\left(\varepsilon_{bw}^{\alpha}-\varepsilon_{i}^{\alpha}\right) &= \left(\varepsilon_{r}^{\alpha}-\varepsilon_{a}^{\alpha}\right)-\theta_s\left(\varepsilon_{s}^{\alpha}-\varepsilon_{a}^{\alpha}\right)-\theta_{TOT}\left(\varepsilon_{i}^{\alpha}-\varepsilon_{a}^{\alpha}\right) && (T<0), \end{aligned} \quad (2)$$

where $\theta_{TOT} = \theta_u + \theta_i$ is the total soil water content, θ_s and θ_i are the volumetric fractions of soil and ice, ε_r is the relative permittivity of the soil as reported by the HydraProbe, ε_{bw} is the permittivity of bulk water (which is temperature dependent), and ε_a and ε_i are the permittivity of air and ice, respectively (which were assumed to be 0.99 and 3.27). The permittivity of soil ε_s and the geometry factor α can be obtained by applying Equation 2 to the ε_r of oven-dried soil. We used a value of 0.55 for α and 4 for ε_s, which correspond to the range of values for loam, silt loam, and sandy soils found by Watanabe and Wake (2009). In Equation 2, θ_{TOT} has to be known in order to determine θ_u. Its initial value can be determined from measurements before freezing of the soil. However, when water infiltrates under frozen soil conditions, θ_{TOT} will have to be updated throughout the time period over which the correction is applied. We adjusted θ_{TOT} by assuming that the infiltrated volume of water during each hourly time step was distributed over the top 0.10 m of the soil core (we refer to the results for a justification of this depth).

With respect to soil temperature, we assumed that the frozen/unfrozen boundary was located at the 0 °C isotherm and that any infiltrating water would refreeze (if the soil was frozen) in the zone of steepest temperature gradient, (Hayashi et al., 2003; Zhao et al., 1997). We used both temperature profiles and temperature gradient profiles to estimate the depth of the infiltration front.

Water may evaporate from frozen soils when they are exposed to the atmosphere and receive sufficient incoming radiation or other energy. We did not measure all environmental variables or mass changes in the columns to quantify evaporation rates during our experiments. However, estimates with the Penman–Monteith equation and evaporation coefficients for bare soil (Allen, Pereira, Raes, & Smith, 1998) suggest that evaporation rates would have been very small: lower than 0.1 mm d^{-1}. We therefore ignore this water balance term in the remainder of the analysis.

2.3 | Field-scale observed snowmelt event

From our core-scale experiments, we determined relationship between antecedent soil moisture and infiltration capacity. We applied these relationship to the hillslope-scale spatial observations of antecedent soil moisture and snowmelt input rates during the 2014 snowmelt period on Hillslope 2 of the Swift Current Hillslopes (Figure 2). The geospatial statistics of mapped SWE, antecedent soil moisture, and snowmelt rates were determined with the gstat package in R Statistical Software (Gräler, Pebesma, & Heuvelink, 2016; Pebesma, 2004; R Core Team, 2016). We calculated the semi-variogram of each dataset and fitted a variogram model to these data to determine the autocorrelation length and source of variance of each variable.

2.3.1 | Antecedent soil moisture

We used a portable Stevens HydraProbe POGO to measure volumetric soil water content at 0 to 0.06 m-depth on a 480-point grid (10 × 10 m spatial resolution) on Hillslope 2 (Figure 2) on October 24, 2013. This date was immediately prior to winter snowfall and freeze-up. We used these data as the antecedent soil moisture conditions for the spring snowmelt season (March 2014) since the soil remained frozen from this date in late October to the commencement of melt in March 2014. The difference between average porosity and

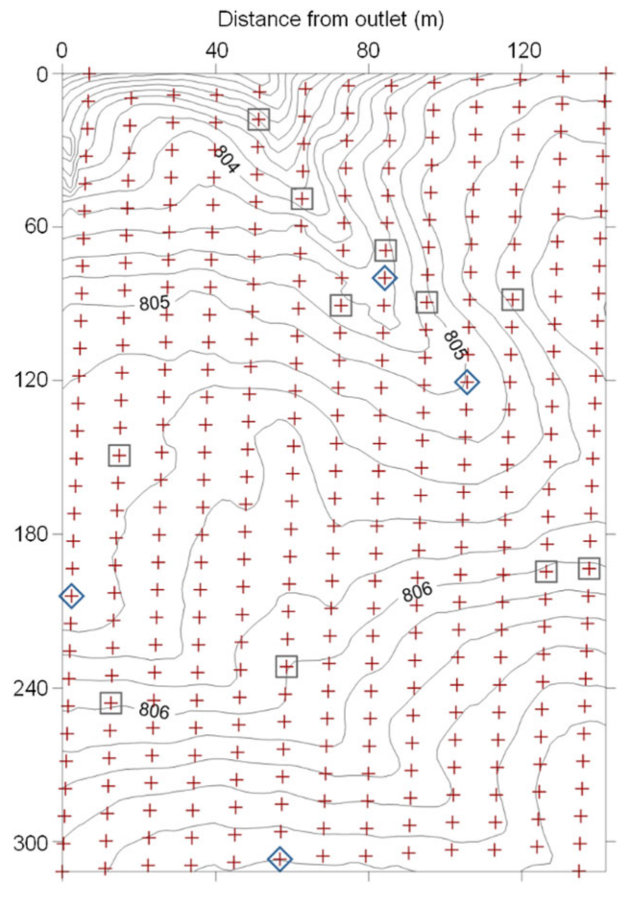

FIGURE 2 Digital elevation map of Hillslope 2 at the Swift Current Hillslopes showing locations of soil moisture profiles (diamond shapes), soil moisture measurements in October 2013 (plus signs), snow cover survey locations (plus signs), and snowmelt rate measurements from snowmelt lysimeters (square shapes)

antecedent soil moisture determined the pre-melt soil water storage capacity (SWSC), that is, the empty pore volume before the start of snowmelt.

2.3.2 | SWE and snowmelt rates

We undertook daily snow surveys to estimate snowmelt rates at a high spatial resolution across Hillslope 2 (Figure 2). We measured snow depth and calculated density and SWE (density was determined by extracting a core of snow, transferring it to a Ziploc® bag, and weighing it on a digital balance, whereas SWE was determined using the density and snow depth measurements), on a 225-point grid (a 10 × 20 m spatial resolution in the lower two-thirds of Hillslope 2, and a 10 × 40 m spatial resolution in the upper third of Hillslope 2). These snow surveys were carried out daily, every morning before any significant melt, through the snowmelt period. Daily ablation could then be estimated at the 225 points:

$$AB_i = SWE_{M,i+1} - SWE_{M,i}, \tag{3}$$

where AB is ablation (mm d^{-1}) on day i, which is the difference between average snow water equivalent SWE_M on day i and day $i + 1$. Assuming relatively minimal ablation by evaporation, sublimation, and wind redistribution during the snowmelt period, then the snow survey data provide an estimate of average daily melt rate at 225 points.

2.4 | Simulation of run-off generation and hydrological connectivity

The goal of the model simulations in this study was not to provide a detailed description of melt and thaw dynamics at the hillslope but rather to investigate the interactions between spatial distributions of hydrological variables. Therefore, we opted to use a conceptual overland flow redistribution model parameterized with observations from the core experiments and field surveys, instead of a fully coupled hydrological and thermal energy transport model (e.g., HydroGeoSphere; Therrien, McLaren, Sudicky, & Panday, 2010).

2.4.1 | Redistribution model

The redistribution model routes water at the soil surface through a complex topography. The basic model creates a database of microdepressions and their contributing areas, based on a detailed digital elevation model (DEM) of a field (Appels, Bogaart, & van der Zee, 2011). When water is present at the soil surface, because of infiltration or saturation excess run-off generation, it fills up microdepressions that spill or merge into other depressions when full (Appels, Bogaart, & van der Zee, 2016). Flowpaths establish as a series of full depressions. The direction of flow on the surface is therefore dependent on the amount of water stored in depressions. For our current purpose, the redistribution model was adapted to contain a subsurface soil storage reservoir, a daily curve of infiltration capacity for each cell of the DEM, and a SWE reservoir for each cell of the DEM. The model captures the effects of spatial distributions of hillslope properties on hydrological connectivity well under a variety of conditions (Appels et al., 2016; Appels, Graham, Freer, & McDonnell, 2015).

The depth of the subsurface soil storage reservoir was set at 0.1 m uniformly throughout the field, based on findings of infiltration depth in the core experiments (results discussed in Section 3.1.2). The fall soil water content, obtained from the field survey in October 2013 (Sections 2.3 and 3.2), determined the soil water storage capacity available in each cell of the DEM.

Model simulations were performed hourly during the 12 nonfrozen hours of the day for a period of 5 days. At the beginning of each day, an updated S_a value was determined for each DEM grid cell from the θ_{TOT} map of the field. The infiltration capacity of each grid cell could then be calculated with the updated S_a and average, constant K_e according to Equation 1. Every hour, a snowmelt rate (uniform throughout the field) was compared to the infiltration capacity. After performing this evaluation for every cell of the DEM, the excess water was routed through the (micro-)topography of the field and ponding locations and levels were determined. The SWE map was updated with the daily amount of melt at each grid cell. The infiltrated amount of water in each cell was added to the subsurface storage reservoir, and the θ_{TOT} map of the field updated. Model outputs include maps of infiltration, θ_{TOT}, ponded water levels, flowpath distribution, and a water balance. Hydrological connectivity was evaluated by plotting surface run-off at the field outlet as a function of the amount of water ponded on the field. This relationship is also known as the relative surface connection function (Antoine, Javaux, & Bielders, 2009).

2.4.2 | Model scenarios

We simulated two soil water content situations, uniform versus spatially distributed θ_{TOT}, and two snowmelt scenarios. The melt rates were obtained from field observations of SWE decline (Section 2.3). From the collection of 225 points, we created a daily melt map for the period March 9 through March 19. In general, these showed higher melt rates at the southern half (top) of Hillslope 2 in the early stages of snowmelt, and then higher melt rates at the northern half (base) of the hillslope towards the end of the snowmelt period. A second series of maps were created by rotating the original interpolated maps by 180° (melt rates are initially highest at the base of the hillslope and then highest at the top of the hillslope later in the snowmelt period).

3 | RESULTS

3.1 | Laboratory experiment

3.1.1 | Surface run-off

Hourly run-off volume and rates increased during the experiments (Figure 3b). In the wet experiment, run-off was generated on all 4 days. However, maximum daily run-off ratios varied widely from a low of 0.1 (at the start of the experiment) to a high of 0.9 (at the end of the experiment; Figure 3c). The total amount of run-off from the wet experiment was 1842 ± 256 ml or 26 mm (average and standard deviation from the three replicates), which equals 52% of the total snowmelt input. In the dry experiment, run-off was not generated from these cores until Day 2, with maximum daily run-off ratios between 0.25 and 0.85 (Figure 3c). The total amount of run-off from the dry

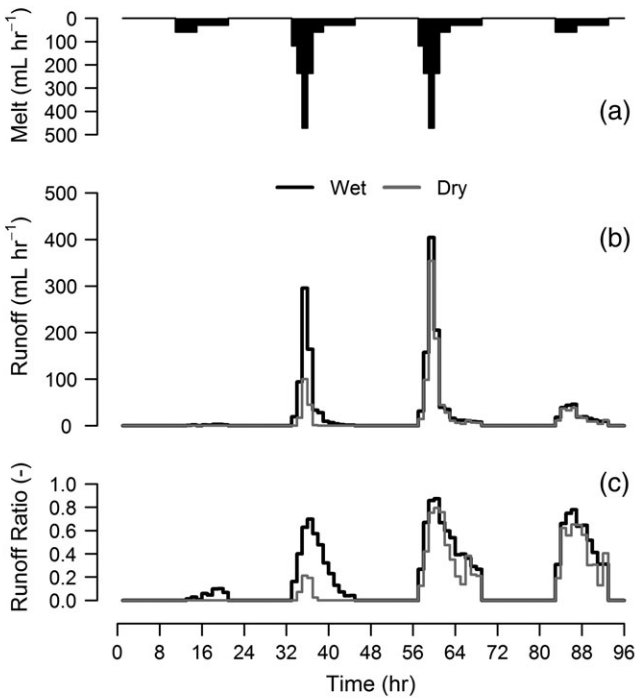

FIGURE 3 (a) Snowmelt, (b) average surface run-off rates, and (c) and average run-off ratios, of Experiments 1 (wet) and 2 (dry)

experiment was 1123 ± 109 ml or 16 mm, which equals 32% of the total snowmelt input.

3.1.2 | Infiltration

Infiltration occurred variably within the cores, with some preferential flow along roots. We found no evidence of deep preferential flow as no brilliant blue was found at depths >0.1 m after the last experiment (Figure 4). Total infiltration into the cores was 24 mm during the wet experiment and 34 mm during the dry experiment. Where the small snowmelt pulse infiltrated mostly and completely (wet and dry

FIGURE 4 Image of excavation of Core 3 at the end of Experiment 2. The top 0.1 m of soil has been removed from the core to reveal limited penetration of the dye into the soil. Note how on the protruding horizontal face of the core (which equates to approximately 30% of its horizontal area) no blue staining can be found

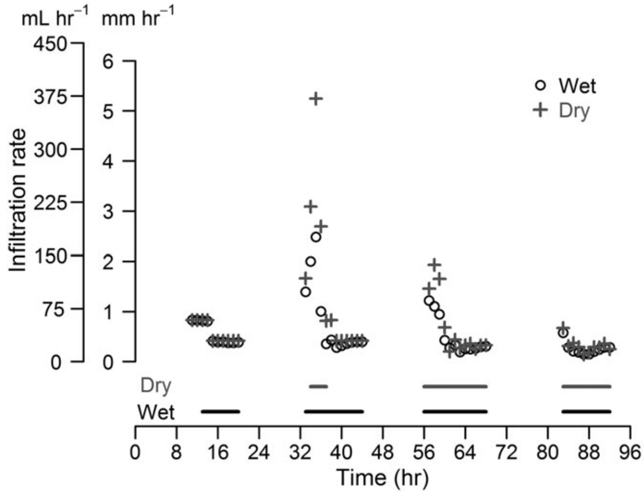

FIGURE 5 Infiltration rates during Experiments 1 (wet) and 2 (dry). The lines at the bottom of the plot indicate when infiltration rates equalled the infiltration capacity of the soil

experiment, respectively) on the first day, only half of that same snowmelt pulse infiltrated on the last day (Figure 5). The infiltration rate (I_R) observed during the experiments was partly controlled by the snowmelt rate (first half of Day 1 of wet experiment; Day 1 and parts of Day 2 of dry experiment); the infiltration capacity (I_C) of the frozen soil during these periods remained therefore unknown. After this period, the I_R was equal to the I_C of the frozen soil controlled the infiltration capacity (I_C) of the frozen soil and run-off was generated. The I_C of the frozen soil did not decrease continuously over the course of the experiments (Figure 5). The redistribution of moisture in the refreezing soil profile between the melt periods allowed for an increase in I_C at the start of each new day. A second, smaller, increase in I_C was observed at the end of Days 3 and 4 when the snowmelt rates decreased. After 56 hr, I_C showed the same dynamics in the wet and dry experiments. Average final I_C was 0.3 mm hr^{-1}.

3.1.3 | Redistribution of water in the soil profile

The HydraProbe II sensors registered a daily liquid water content (θ_u) that was dynamic at all depths in the cores (Figure 6). Soil temperature fluctuated between −1 and 0 °C during infiltration events, a transitional temperature range in which the rapidly changing relative permittivity of a partially frozen soil hampers the accurate estimation of water and ice ratios. Small (<0.02 m^3 m^{-3}) increases and decreases were the result of these temperature fluctuations. In a frozen soil, the liquid volumetric water content is mostly a result of the presence of small particles with a large surface area and not of the total volumetric water content of the soil (Watanabe & Wake, 2009). The initial soil water content in Figure 6 therefore did not represent the volumetric water content before freeze up but particle and pore heterogeneity of the soil in the columns.

The larger soil water content dynamics in the top of the cores (θ_{TOP}) on Days 2, 3, and 4 represent the combination of infiltration and thawing/refreezing (Figure 6a,c). The peak on Day 2 could be attributed completely to newly infiltrating water. During the wet experiment, the average soil water content increase in the cores was

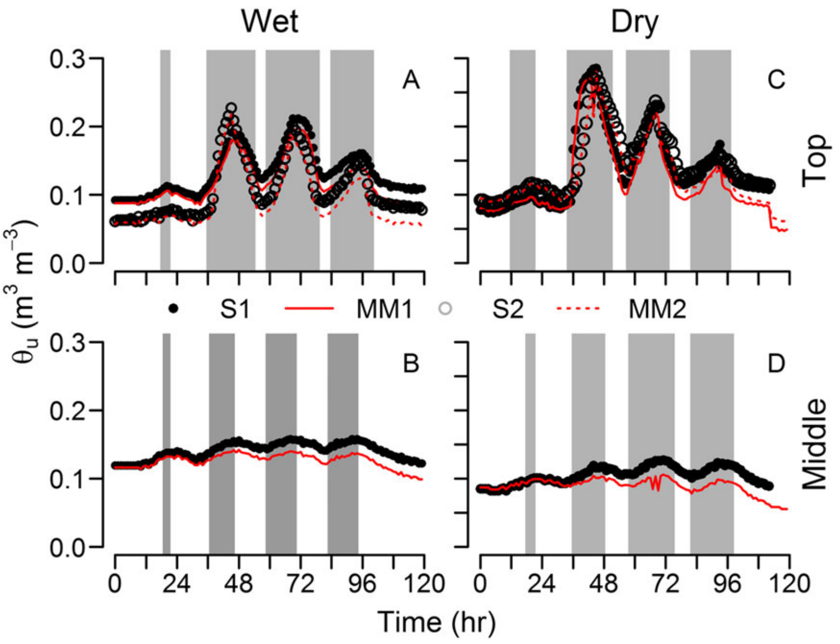

FIGURE 6 Hourly unfrozen volumetric water content readings from HydraProbe II sensors in one core (columns) at two depths (rows) during the 4 days of each experiment and one extra day afterwards. Points (S1 and S2) indicate raw values, red lines the values calculated with the mixing model (MM1, MM2). Two sensors were positioned at the top of each core, one in the middle. The grey background shading indicates hours when the soil temperature measured by the sensors was >−1 °C

0.12 ± 0.03 m^3 m^{-3}. It reached 0.19 ± 0.01 m^3 m^{-3} during the dry experiment. This water refroze overnight, resulting in a sharp decrease to a soil water content of 0.02 ± 0.01 m^3 m^{-3} higher than the initial soil water content. The peaks of Days 3 and 4 represent two more cycles of thaw and freeze as well as further diffusion of the infiltration front. Infiltration rates and volumes were lower on these days and the peak soil water content lower than that of Day 2 as a result. A smaller infiltration-induced bump in soil water content was observed at the middle positions in all cores (θ_{MID}) during the wet experiment and two cores during the dry experiment (Figure 6b,d). At the bottom positions, no infiltration-induced fluctuations were observed in the HydraProbe II soil water content signals (θ_{BASE}). At the end of the experiment, all introduced water refroze.

Soil temperatures in the cores fluctuated on a daily basis in the entire profile of the columns (Figure 7a,b) because of the limited thermal mass of the cores. The temperature patterns varied between the experiments given the same air temperature conditions and snowmelt input over time. Cores 1 and 2 remained frozen throughout the wet experiment. In the dry experiment, the top 0.02 to 0.03 m reached 0.1 °C, and water was infiltrating (Cores 1 and 2). Soil thawing from the freely draining, uninsulated bottom of the cores was observed in Core 1 (dry experiment) and Core 3 (both wet and dry experiments; not shown in Figure 7, which only shows the temperature fluctuations in the top half of the core). However, as expected at the beginning of the experiment, the infiltration front did not reach the thawed zone near the bottom of the cores. Core 3 reached temperatures >0 °C during Days 2, 3, and 4 of both experiments as the infiltration front moved downward. This was most apparent in the dry experiment.

The downward moving of a thawing (infiltration) front is driven by the external energy input from the surface, which moves by conduction through the unfrozen soil layer above the front. The thawing front speeds were 11 mm d^{-1} for the wet and 17 mm d^{-1} for the dry experiment. Refreezing is indicated by blue colours in the temperature gradient profiles (Figure 7c,d), and a potential impediment to any deeper infiltration of the snowmelt water. In the dry experiment, refreezing occurred at depths of <0.08 m, whereas refreezing during the wet experiment occurred at depths of <0.06 m. Because infiltration diminished through the course of the 4-day experiment, the zone of refreezing narrowed.

3.2 | Hillslope spatial variability of soil water content, SWE, and snowmelt rates

The shallow volumetric soil water content in October 2013 ranged between 0.11 and 0.30 m^3 m^{-3}, with an average of 0.18 m^3 m^{-3} (Figure 8). The antecedent wetness of the soil cores in our laboratory experiment (0.11 and 0.18 m^3 m^{-3}) bounds 59% of the data points in the field. There was no spatial correlation between topographical features (depressions, steep slopes, and gullies) and shallow soil water content.

The last snow survey before spring melt was performed on March 8, 2014 (Figure 9). The field average SWE was 74.7 ± 19.4 mm. The largest amounts of SWE were found along the berm at the north end of the field and at the high, steep end of the gully that cuts through the field in a northeast direction. This was a result of wind blowing snow against the raised berm and shelter from wind and ablation throughout the winter, respectively.

Snowmelt rates (measured as daily SWE loss rates) varied considerably across the hillslope (Figure 10). At any given day in the 11-day period, 20% to 60% of the 225 points did not experience any melt, and maximum rates varied between 40 mm d^{-1} on March 9 and 70 mm d^{-1} on March 16. The sum of median daily SWE losses amounted to 53.4 mm, similar to the 52 mm applied in the lab experiments.

The geospatial statistics of these hydrological variables are presented in Table 1. The range of the fitted models, that is, the distance beyond which values are no longer autocorrelated, increased from SWE distribution, to elevation, to antecedent soil moisture condition. The ranges of the snowmelt rate distributions started larger than that of the elevation, decreasing mid-period and increasing again at the end.

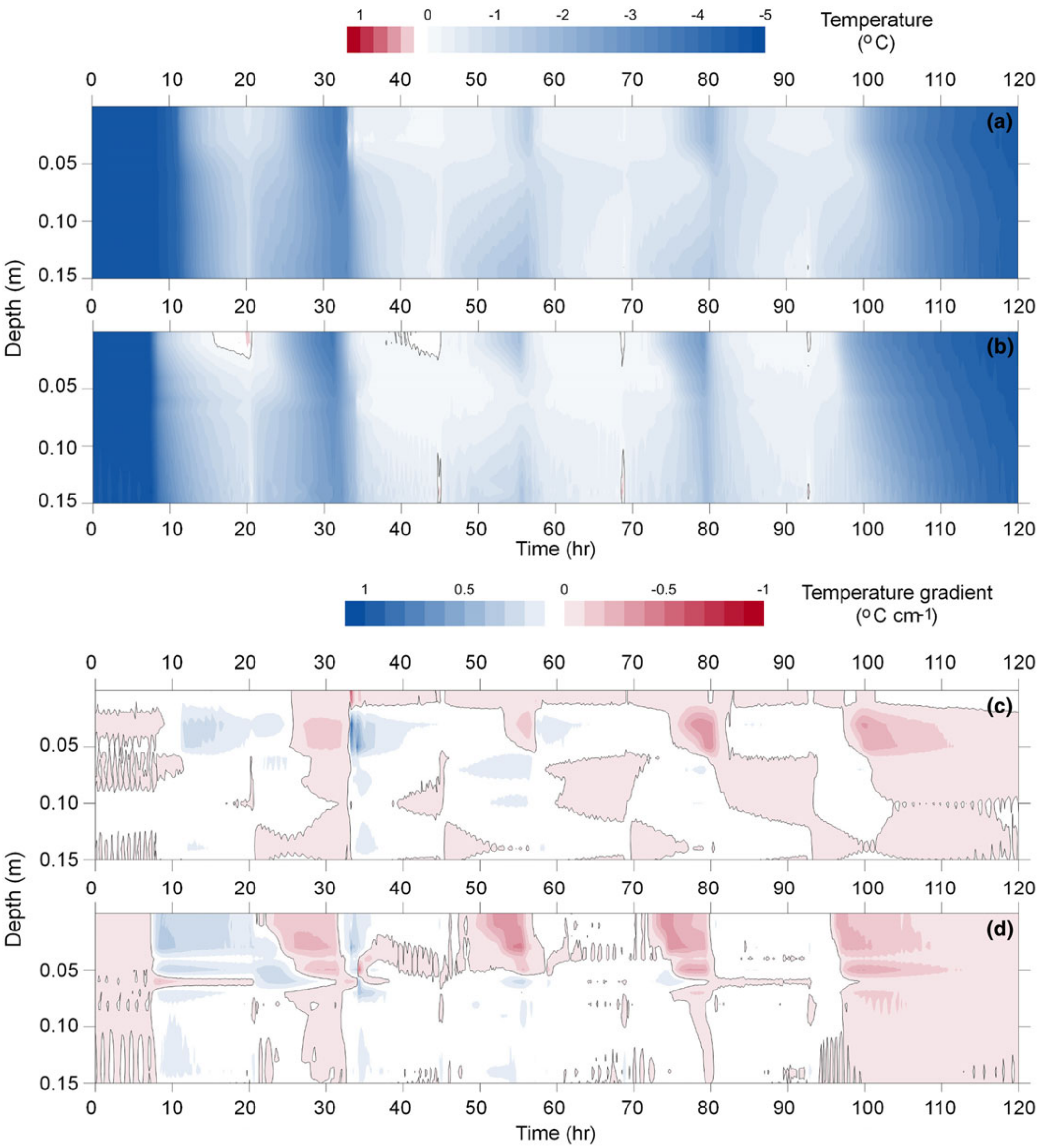

FIGURE 7 Soil temperature profiles of Core 2 during (a) Experiment 1 (wet) and (b) Experiment 2 (dry). Soil temperature gradients of Core 2, where reds indicate a warming gradient down core and blues indicate a cooling gradient down core, during (c) Experiment 1 (wet) and (d) Experiment 2 (dry)

On Days 9 and 11, and in the spatial distribution of antecedent moisture, the nugget amounted to 77%, 73%, and 70% of the total semivariance, respectively. This indicates that for these patterns, the majority of variance originated at distances smaller than the distances between the monitoring points (here, ~10 m), or resulted from measurement errors. The latter is less likely for the antecedent soil moisture measurements which leads us to conclude that most variability of antecedent soil moisture occurred at distances smaller than 10 m.

3.3 | Simulations of run-off generation and hydrological connectivity

Based on the results of the laboratory experiment, six sorptivity (S_a) values were obtained from fitting the infiltration model (Equation 1) to the six infiltration curves (Figure 5) that generated surface run-off. Figure 11 shows these values as plotted as a function of estimated total water content θ_{TOT} (ice plus liquid water) in the top 0.10 m of the cores. A linear model fitted to these points provided an estimate of S_a for all moisture values found in the field before freeze-up and new θ_{TOT} for the duration of the simulations. In the process of fitting the infiltration model, an average value of 0.06 mm hr^{-1} was obtained for K_e.

The simulated spatial pattern of cumulative infiltration and timing of ponding and run-off was not sensitive to the spatial distribution of total SWE (results not shown). Infiltration patterns were affected by the spatial distribution of moisture before freeze-up, but total cumulative infiltration and timing of ponding and run-off were not (Figure 12). Similarly, changes to the spatial distribution of snowmelt rates did not affect total cumulative infiltration (Figure 12a). We expressed hydrological connectivity as a relative surface connection function (Antoine et al., 2009). Figure 12c shows these functions for the four scenarios of varying spatial distributions of snowmelt and pre-freeze-up moisture content. The distribution of pre-freeze-up moisture content did not affect the hydrological connectivity, but the distribution of snowmelt rates changed the filling rates of the various depressions in the

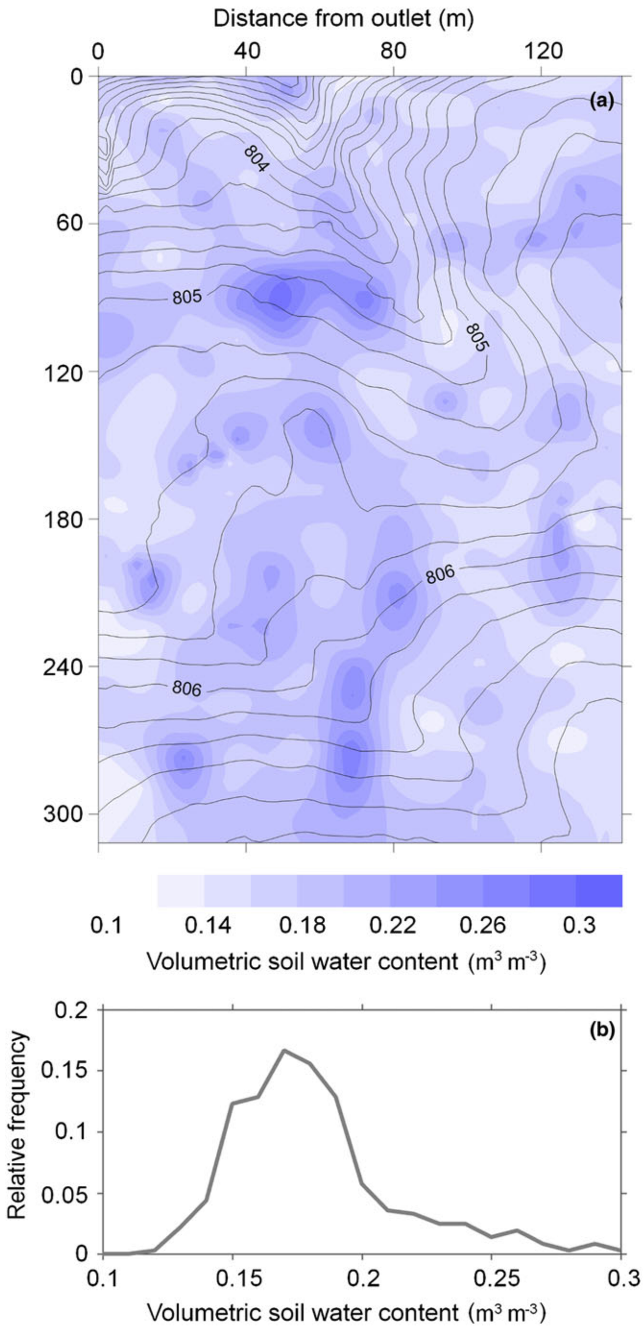

FIGURE 8 (a) Map of shallow soil moisture distribution before freeze-up in October 2013, and (b) frequency distribution of the values

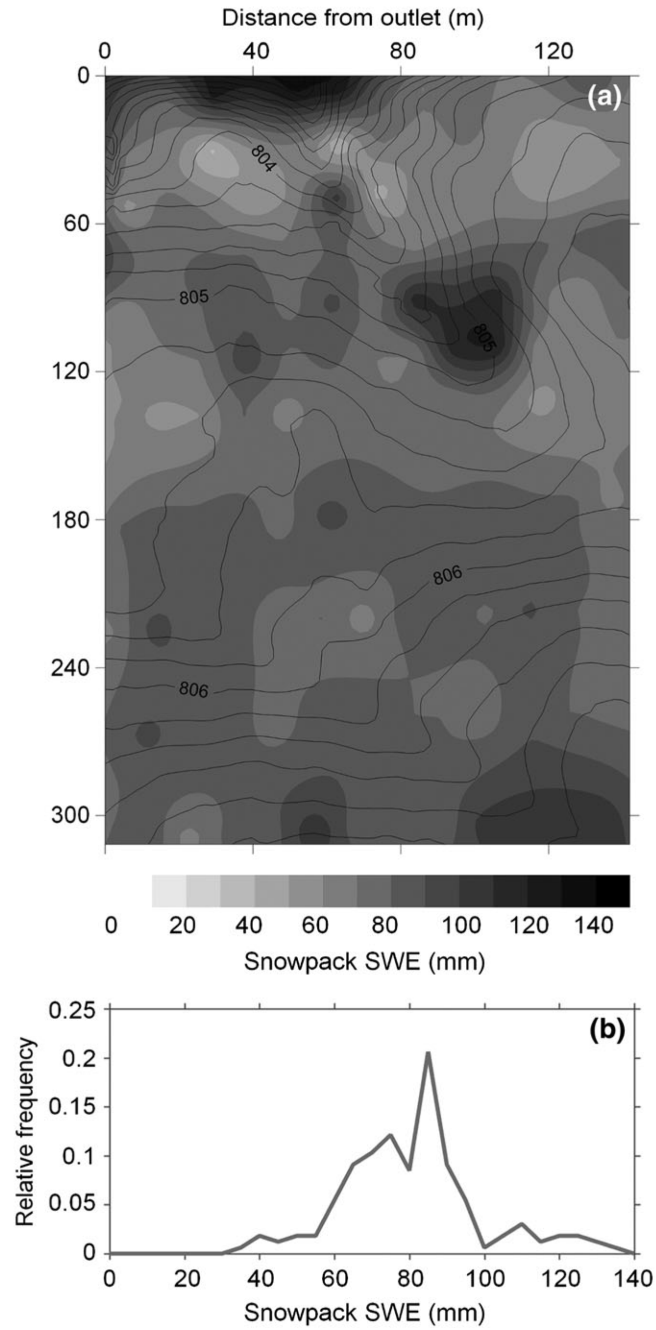

FIGURE 9 (a) Map of snowpack water equivalent distribution on March 8, 2014, before spring melt, and (b) frequency distribution of the values

field and the flowpath development along the hillslope. The rotated series of snowmelt rate maps (where melt rates are initially highest at the base of the hillslope, and then highest at the top of the hillslope later in the snowmelt period) generated less cumulative run-off (Figure 12b) but triggered run-off at lower cumulative hillslope storage (Figure 12c), as compared to the observed snowmelt maps.

4 | DISCUSSION

4.1 | Infiltration-run-off partitioning in lab and field

Our 4-day lab experiments showed that infiltration and refreezing of infiltrating melt water occurred within a shallow (c. 0–0.10 m) layer. The majority of infiltration refreezing—induced from observed soil temperatures—did not occur immediately following snowmelt application but rather overnight when the air temperature was lowered to simulate observed diurnal temperature fluctuations from the field. The resulting opportunity for redistribution of infiltrated water before refreezing, caused a high infiltration capacity at the start of each day, followed by a decrease during the day. This start-of-day infiltration capacity lowered as the melt period progressed and the SWSC filled. Such a damping oscillating process has been observed in field and modelling studies of an Alpine permafrost site (Scherler, Hauck, Hoelzle, Stähli, & Völksch, 2011).

A frozen soil dominated by capillary flow has a lower SWSC and infiltration capacity than a nonfrozen soil, because refreezing causes

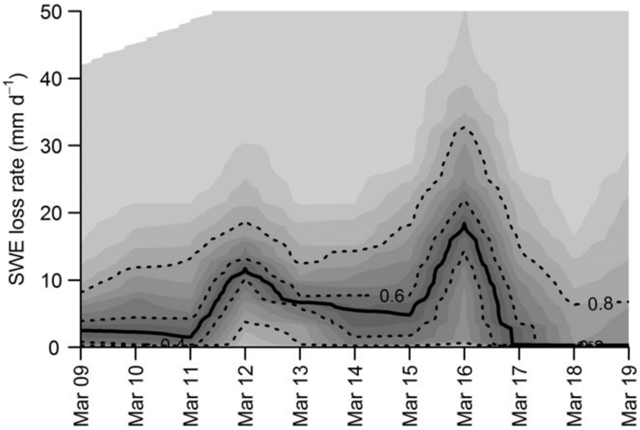

FIGURE 10 Quantiles (20%, 40%, 50%, 60%, and 80%) of daily snowpack water equivalent loss at the hillslope during the 2014 melt period. Grey shading indicates 5% increments

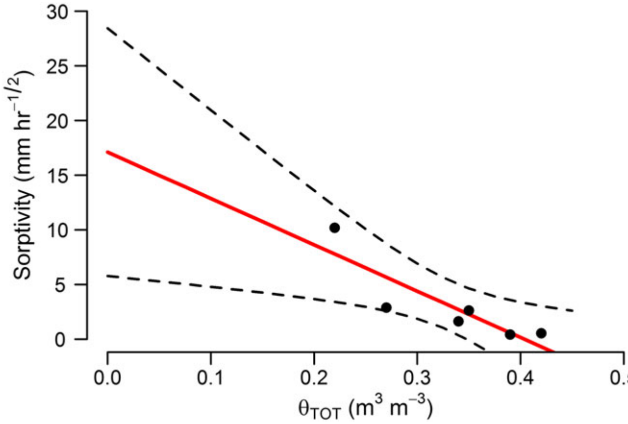

FIGURE 11 Linear model of apparent sorptivity S_a of the Philip infiltration equation as a function of total water and ice content. Points are the values obtained from the lab experiment. The dashed lines indicate the 95% confidence interval

ice to block the interconnectivity of soil pores (Fourie, Barnes, & Shur, 2007; Gray et al., 2001; Kane, 1980; Kane & Chacho, 1990). Specifically, for a frozen, fine-textured mineral soil, the average storage potential is approximately 60% of its air-filled pore spaces at the start of infiltration (Gray et al., 2001) and infiltration volumes may be reduced by >75% in the presence of ice-filled pores (Kane, 1980). Our results showed that although the initial storage capacity of the shallow layer and average infiltration penetration depth depended on the initial soil water content, the shallow refreezing created saturated conditions at the surface in both the dry and wet cores and limited infiltration to similar levels (0.3 mm hr^{-1}) 2 days into the experiment.

If we extrapolate the core findings to the hillslope-scale, it is clear that total pre-melt SWE far exceeded the antecedent soil water storage capacity (by a factor of 5–10). The range of variability of infiltration as a result of antecedent moisture variability was then much smaller than the variability induced by nonponding versus ponding locations. With an average (simulated) water level in depressions of 0.04 m (max 0.11 m), total infiltration under ponded locations was twice that of nonponding locations. This illustrates that a hillslope is more than a sum of infiltrating columns and emphasizes the importance of depression-focused infiltration for groundwater recharge on the Prairies (Berthold, Bentley, & Hayashi, 2004; Hayashi et al., 2003). However, in terms of connectivity and run-off generation, this spatial variability only had small effects, because ponded water was equal to only 1 mm across the hillslope (out of an average of 75 mm SWE before melt).

TABLE 1 Properties of geostatistical models fitted to hydrological observations of the 2014 snowmelt period

	Variogram model			
Observation	Type	Nugget	Sill	Range (m)
Elevation (m)				
	Gaussian	0.0088	0.159	48
Snowpack water equivalent (mm)				
	Spherical	15	316	29
Antecedent soil moisture (m^3 m^{-3})				
	Spherical	0.07	0.03	77
Melt rate (mm d^{-1})				
Day 1	Spherical	0	35	51
Day 2	Spherical	0	48	64
Day 3	Spherical	3	56	75
Day 5	Spherical	35	51	27
Day 7	Spherical	35	103	44
Day 8	Spherical	39	253	38
Day 9	Spherical	75	98	68
Day 11	Spherical	105	144	62

Note. Models could not be successfully fitted to all melt rate datasets (Days 4, 6, and 10). The units of the nugget and sill are equal to that of the observation.

Although preferential flow to depth has been shown to be important for infiltration into frozen prairie soils, especially on grasslands (Granger et al., 1984; Hayashi et al., 2003), it was not observed in our laboratory experiments. This is not to say such flowpaths do not occur on our site, even though prairie agricultural sites have been shown by others to feature shallower and reduced infiltration than prairie grasslands (van der Kamp, Hayashi, & Gallén, 2003). It is possible that our intact soil core extraction locations exhibited fewer preferential flowpaths than was typical of the larger hillslope. This could have resulted in an underestimation of infiltration capacity in the field. However, refreezing of infiltration may also occur in macropores, as observed by Watanabe and Kugisaki (2017), limiting infiltration capacity in a similar fashion as in the soil matrix. Under ponded conditions, the reduction of permeability may be partly overcome by larger head gradients (Scherler et al., 2011).

4.2 | Snowmelt hydrological connectivity at the Swift Current site

Previous work at the Swift Current site has shown that microtopographic and mesotopographic features fix locations of ponding during snowmelt (Coles & McDonnell, 2017). The timing and filling rates of ponding at these locations are a function of the difference between melt rate and infiltration capacity, as well as the difference between soil water storage capacity and the amount of water in the snowpack. These hydrological variables all have their own spatial

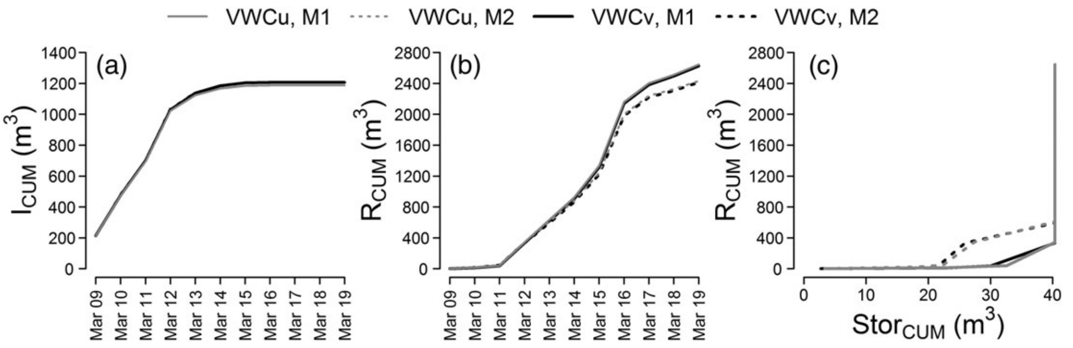

FIGURE 12 (a) Simulated cumulative infiltration and (b) cumulative surface run-off of the hillslope for the four combinations of initial moisture (uniform **VWCu** and spatially distributed **VWCv**) and snow melt (observed **M1** and 180° rotated **M2**). Panel (c) quantifies hydrological connectivity by plotting surface run-off as a function of amount of water stored at the soil surface

distribution at the hillslope scale and specific effects on patterns of ponding and run-off generation, that is, hydrological connectivity. These effects obscure the singular control of the frozen aspect of soil on run-off response and infiltration distribution (Hayashi, 2013) and are the main reason why application of point-scale understanding of infiltration into frozen soil to prediction at the hillslope- and catchment-scales has been so difficult.

Gray et al. (2001) showed that antecedent moisture is the primary control on infiltration into frozen prairie soils, but here, we have found that the *spatial distribution* of antecedent moisture is not a controlling factor when we move up to the hillslope-scale. Our results indicate that this is due to (a) the magnitude of the soil moisture reservoir compared to that of the snowpack, and also to (b) the correlation characteristics of the spatial pattern of antecedent moisture compared to the correlation characteristic of the spatial pattern of topography (Table 1). Although antecedent soil moisture conditions govern the infiltration capacity and the soil water storage capacity, any differences between locations in the field disappeared during the first 3 days of the melt period. In addition, 70% of antecedent moisture variability occurred at distances smaller than that of the measurement points (nugget was large), which was shorter than that of the topography (Table 1). This implies that within each pond or flowpath, all moisture values have an equal chance of being present; in order for run-off to be generated, the infiltration capacity or SWSC of all will need to have been overcome. The rates at which depressions fill up will be controlled more by the geometry of depressions and their contributing areas than by the exact soil water content pattern. As a result, simulated connectivity patterns and run-off ratios were similar for spatially distributed and uniform hillslope-averaged antecedent soil moisture. This suggests that spatially variable soil water content data are not important for hillslope-scale hydrological modeling and prediction on the Prairies but rather hillslope-averaged data are sufficient.

SWE patterns were not important to the connectivity pattern for similar reasons: autocorrelation distance was smaller than that of elevation (i.e., all possible values could be present in a topographic feature). In addition, because the amount of SWE was larger than both soil water storage capacity (by a factor of 5–10) and surface depression storage capacity (by a factor of 15–30), nowhere on the hillslope did supply volume limit run-off generation.

The spatial pattern of snowmelt rates did affect run-off and connectivity: larger autocorrelation distances than elevation and a relatively small nugget meant that the topographical features on the hillslope (depressions or sloping areas) received largely the same melt rates. More "fill" variability occurred between than within topographical features. In our simulation example, the rotation of the snowmelt distribution map resulted in larger areas of the hillslope with direct connections to the hillslope outlet, whereas the depressions in the southern half were still filling. The switch to spatial patterns with shorter autocorrelation distances halfway into the melt period did not significantly affect the connectivity dynamics, because at this point in time, all depressions were full and all flowpaths had been established.

4.3 | Wider implications for hillslope connectivity on the Prairies

Our findings indicate how the hierarchy of spatially variable controls will shift between locations and from winter to winter. The 2013–2014 winter on Hillslope 2 at the Swift Current site featured a larger snowpack than the long-term average for the site (in part due to the snow trapping effects of a high stubble residue on the hillslope) and ponding and run-off dynamics were controlled by the spatial variability of snowmelt rates. Average and below-average SWE conditions may switch that to a situation of supply limitation. Feedbacks play an important role here: less SWE may affect the level of soil frost and soil thaw during the melt season and consequently infiltration rates and volumes (Quinton, Bemrose, Zhang, & Carey, 2009).

In steeper catchments, topography may control the spatial distribution of snow as well as that of melt rates and antecedent moisture conditions. As a result, the strength of the patterns conspire to one preferential response (Williams, McNamara, & Chandler, 2009). Coles and McDonnell (2017) hypothesized that soil water content may only affect ponded water development and flowpath formation in the snowmelt season if a more undulating site froze very soon after rainfall (e.g., side slopes freeze dry and swales freeze wet) thus leaving a more organised (less random) spatial pattern of soil water content.

We suggest that, in general, hillslope-wide hydrological connectivity on the Prairies is easier to achieve during spring snowmelt than other large hydrological events (e.g., a summer and convective rainstorm) because the contrast between input depths (i.e., precipitation amount) and storage volume (e.g., soil water storage capacity) as well as the contrast between input rates and infiltration rates are larger in spring than in summer. Small snowpacks and/or slow melt rates would be limits to hillslope-wide connectivity within spring snowmelt events. Such conditions are not uncommon. Over the 1962–2013 period, annual snowpack SWE at the Swift Current site varied between 0 (nonexistent) and 121 mm, with a long-term mean of 33 mm (Coles, 2017). In winters with small snowpacks, the effects of SWE and soil water content distribution on ponding and connectivity dynamics will become more pronounced. In addition, if soil thaw were to coincide with the snow melt period, as it currently does occur further south in the Prairie region, distributions of soil water content may gain a new importance.

5 | CONCLUSIONS

We combined core-scale laboratory experiments and field observations into model simulations to investigate the controls on infiltration-run-off partitioning and hydrological connectivity during snowmelt on a frozen prairie hillslope. Our 4-day laboratory experiments showed that infiltration and refreezing of infiltrating melt water occurred within a shallow (c. 0–0.10 m) layer. Antecedent moisture conditions of the frozen soil affected the infiltration rates by, in the case of wetter soils, limiting the initial soil storage capacity and infiltration front penetration depth. However, the shallow refreezing created saturated conditions at the surface in both the dry and wet soil core experiments, which meant that by 56 hr into both experiments, infiltration was occurring at similar rates (0.3 mm hr^{-1}) despite differing antecedent moisture conditions.

At the hillslope-scale, infiltration-run-off partitioning would likely have varied, depending on antecedent moisture conditions, in the first 2 days of the melt period. Following this, infiltration rates would have been limited throughout the hillslope due to shallow refreezing of infiltrated water. We showed that the development of hydrological connectivity at the hillslope-scale during the 2014 spring melt was controlled by the spatial variability of snowmelt rates and then routed by the topographic controls as shown previously by Coles and McDonnell (2017). The spatial patterns of snowpack SWE and antecedent soil moisture were unimportant. This is because antecedent moisture variability and SWE variability occurred at distances shorter than that of the topographic variability. In addition, SWE was much larger than both soil water storage capacity (by a factor of 5–10) and surface depression storage capacity (by a factor of 15–30), so nowhere on the hillslope did supply volume limit run-off generation. We hypothesise that during the melt of small snowpacks, the effects of SWE and antecedent soil moisture distribution on ponding and connectivity will become more pronounced.

Our findings extend Coles and McDonnell's (2017) description of the fill and spill mechanism of run-off generation at this site during spring snowmelt 2014—which showed that surface microdepression and mesodepression must fill with ponded water before they can spill and connect. However, their work was not able to resolve the effects of antecedent soil moisture and melt rates on spatial variation of infiltration and the ponding of water (a previous step to the fill and spill of surface depressions in the generation of run-off at this site), which we have been able to explore here. Therefore, although the fill and spill of surface depressions remains fundamental to the generation of run-off at the hillslope outlet, we have shown that there is an earlier "fill" step (but importantly no accompanying "spill" step): that the thin surface soil layer first wets-up, refreezes, and pseudo-saturates (i.e., "fills"), and only then does ponded water generate above the frozen soil layer, and filling and spilling of microscale and mesoscale topographic depressions occur.

The model simulations presented in this paper were simple and empirical, powered with our laboratory findings. The conceptual nature of the model prevents it from being used for the investigation of alternative soil freeze–thaw dynamics or predictions of response under climate change. A more physically realistic model (e.g., HydroGeoSphere or SUTRA) would have to be used to explore a mechanistic explanation of the infiltration-run-off partitioning into frozen ground under such conditions. Finally, here, we explained the hierarchy of spatial controls on snowmelt-run-off connectivity using geostatistical properties (i.e., autocorrelation lengths). With the increasing popularity of unmanned aerial vehicles, such patterns could be investigated in more detail in the future.

ACKNOWLEDGMENTS

We thank Marijn Piet for her work during an earlier set of infiltration experiments that formed the basis of the laboratory experiments described in this paper. We also thank Evan Powell for his assistance with extracting the soil cores.

ORCID

Willemijn M. Appels http://orcid.org/0000-0001-9140-1122
Anna E. Coles http://orcid.org/0000-0001-8353-9332

REFERENCES

Allen, R. G., Pereira, L. S., Raes, D., & Smith, M. (1998). Crop evapotranspiration - Guidelines for computing crop water requirements (FAO Irrigation and drainage paper No. 56). Rome: FAO - Food and Agriculture Organization of the United Nations.

Antoine, M., Javaux, M., & Bielders, C. (2009). What indicators can capture runoff-relevant connectivity properties of the micro-topography at the plot scale? *Advances in Water Resources*, *32*(8), 1297–1310.

Appels, W. M., Bogaart, P. W., & van der Zee, S. E. A. T. M. (2011). Influence of spatial variations of microtopography and infiltration on surface runoff and field scale hydrological connectivity. *Advances in Water Resources*, *34*(2), 303–313.

Appels, W. M., Bogaart, P. W., & van der Zee, S. E. A. T. M. (2016). Surface runoff in flat terrain: How field topography and runoff generating processes control hydrological connectivity. *Journal of Hydrology*, *534*, 493–504. https://doi.org/10.1016/j.jhydrol.2016.01.021

Appels, W. M., Graham, C. B., Freer, J. E., & McDonnell, J. J. (2015). Factors affecting the spatial pattern of bedrock groundwater recharge at the hillslope scale. *Hydrological Processes*, *29*(21), 4594–4610. https://doi.org/10.1002/hyp.10481

Baker, J. M. (2006). Water Relations in Frozen Soil. In R Lal. (Ed.), *Encyclopedia of Soil Science* (*Volume* 2) (pp. 1858-1859). New York: Taylor & Francis.

Bayard, D., Stähli, M., Parriaux, A., & Flühler, H. (2005). The influence of seasonally frozen soil on the snowmelt runoff at two Alpine sites in southern Switzerland. *Journal of Hydrology*, *309*, 66–84.

Berthold, S., Bentley, L. R., & Hayashi, M. (2004). Integrated hydrogeological and geophysical study of depression-focused groundwater recharge in the Canadian Prairies. *Water Resources Research*, *40*, W06505. https://doi.org/10.1029/2003WR002982

Birchak, J. R., Gardner, C. G., Hipp, J. E., & Victor, J. M. (1974). High dielectric constant microwave probes for sensing soil moisture. *Proceedings of the IEEE*, *62*(1), 93–98.

Coles, A. E. (2017). Runoff generation over seasonally-frozen ground: Trends, patterns, and processes. Ph.D. Thesis. Saskatoon: University of Saskatchewan.

Coles, A. E., McConkey, B. G., & McDonnell, J. J. (2017). Climate change impacts on hillslope runoff on the northern Great Plains, 1962-2013. *Journal of Hydrology*. https://doi.org/10.1016/j.jhydrol.2017.05.023

Coles, A. E. & McDonnell, J. J. (2017). Fill and spill drives runoff connectivity over frozen ground, Manuscript under review with Journal of Hydrology.

Fang, X., & Pomeroy, J. W. (2007). Snowmelt runoff sensitivity analysis to drought on the Canadian prairies. *Hydrological Processes*, *21*, 2594–2609. https://doi.org/10.1002/hyp.6796

Flury, M., Flühler, H., Jury, W. A., & Leuenberger, J. (1994). Susceptibility of soils to preferential flow of water: A field study. *Water Resources Research*, *30*(7), 1945–1954.

Fourie, W. J., Barnes, D. L., & Shur, Y. (2007). The formation of ice from the infiltration of water into a frozen coarse grained soil. *Cold Regions Science and Technology*, *48*(2), 118–128. https://doi.org/10.1016/j.coldregions.2006.09.004

Gräler, B., Pebesma, E., & Heuvelink, G. (2016). Spatio-temporal Interpolation using gstat. *The R Journal*, *8*(1), 204–218.

Granger, R., Gray, D., & Dyck, G. E. (1984). Snowmelt infiltration to frozen prairie soils. *Canadian Journal of Earth Sciences*, *21*(6), 669–677.

Gray, D. M., Landine, P. G., & Granger, R. J. (1985). Simulating infiltration into frozen Prairie soils in streamflow models. *Canadian Journal of Earth Sciences*, *22*(3), 464–472.

Gray, D. M., Norum, D. I., & Granger, R. J. (1984). The prairie soil moisture regime: fall to seeding. Presented at: Optimum Tillage Challenge Workshop, p17899.

Gray, D. M., Toth, B., Zhao, L., Pomeroy, J. W., & Granger, R. J. (2001). Estimating areal snowmelt infiltration into frozen soils. *Hydrological Processes*, *15*, 3095–3111.

Gupta, H. V. & Sorooshian, S. (1997). The challenges we face: panel discussion on snow. In S. Sorooshian, H. V. Gupta, & J. C. Rodda (Eds.) *Land Surface Processes in Hydrology: Trials and Tribulations of Modeling and Measuring*. *NATO ASI Series* (Vol. I 46) (pp. 183-187). Verlag Berlin Heidelberg New York: Springer.

Hansson, K., Šimůnek, J., Mizoguchi, M., Lundin, L., & van Genuchten, M. T. (2004). Water flow and heat transport in frozen soil: numerical solution and freeze-thaw applications. *Vadose Zone Journal*, *3*, 693–704. https://doi.org/10.2136/vzj2004.0693.

Hayashi, M. (2013). The Cold Vadose Zone: Hydrological and Ecological Significance of Frozen-Soil Processes. *Vadose Zone Journal*, *12*(4). https://doi.org/10.2136/vzj2013.03.0064.

Hayashi, M., van der Kamp, G., & Schmidt, R. (2003). Focused infiltration of snowmelt water in partially frozen soil under small depressions. *Journal of Hydrology*, *270*(3–4), 214–229. https://doi.org/10.1016/S0022-1694(02)00287-1

Ireson, A. M., van der Kamp, G., Ferguson, G. A. G., Nachson, U., & Wheater, H. S. (2013). Hydrogeological processes in seasonally frozen northern latitudes: Understanding, gaps and challenges. *Hydrogeology Journal*, *21*, 53–66. https://doi.org/10.1007/s10040-012-0916-5

Ishikawa, M., Zhang, Y., Kadota, T., & Ohata, T. (2006). Hydrothermal regimes of the dry active layer. *Water Resources Research*, *42*, W04401.

Iwata, Y., Hayashi, M., Suzuki, S., Hirota, T., & Hasegawa, S. (2010). Effects of snow cover on soil freezing, water movement, and snowmelt infiltration: A paired plot experiment. *Water Resources Research*, *46*, W09504.

Jansson, P.-E., & Karlberg, L. (2001). *Coupled heat and mass transfer model for soil-plant-atmosphere systems*. Stockholm: Royal Institute of Technology, Department of Civil and Environmental Engineering.

Kane, D. L. (1980). Snowmelt infiltration into seasonally frozen soils. *Cold Regions Science and Technology*, *3*, 153–161. https://doi.org/10.1016/0165-232X(80)90020-8

Kane, D. L., & Chacho, E. F. (1990). Frozen ground effects on infiltration and runoff. In W. L. Ryan, & R. D. Crissman (Eds.), *Cold regions hydrology and hydraulics* (pp. 259–300). New York: American Society of Civil Engineers.

Kane, D. L., Hinkel, K. M., Goering, D. J., Hinzman, L. D., & Outcalt, S. I. (2001). Non-conductive heat transfer associated with frozen soils. *Global and Planetary Change*, *29*, 275–292.

Kane, D. L., & Stein, J. (1983). Water movement into seasonally frozen soils. *Water Resources Research*, *19*(6), 1547–1557.

Kane, D. L., & Stein, J. (1984). Plot measurements of snowmelt runoff for varying soil conditions. *Geophysica*, *20*(2), 123–135.

Kitterød, N. O. (2008). Focused flow in the unsaturated zone after surface ponding of snowmelt. *Cold Regions Science and Technology*, *53*(1), 42–55.

Li, L., & Simonovic, S. P. (2002). System dynamics model for predicting floods from snowmelt in North American prairie watersheds. *Hydrological Processes*, *16*, 2645–2666.

Lilbæk, G., & Pomeroy, J. W. (2010). Laboratory evidence for enhanced infiltration of ion load during snowmelt. *Hydrology and Earth System Sciences*, *14*, 1365–1374.

Ling, F., & Zhang, T. (2004). A numerical model for surface energy balance and thermal regime of the active layer and permafrost containing unfrozen water. *Cold Regions Science and Technology*, *38*(1), 1–15.

McCauley, C. A., White, D. M., Lilly, M. R., & Nyman, D. M. (2002). A comparison of hydraulic conductivities, permeabilities and infiltration rates in frozen and unfrozen soils. *Cold Regions Science and Technology*, *34*(2), 117–125. https://doi.org/10.1016/S0165-232X(01)00064-7

McConkey, B. G., Ulrich, D. J., & Dyck, F. B. (1997). Slope position and subsoiling effects on soil water and spring wheat yield. *Canadian Journal of Soil Science*, *77*, 83–90.

Moghadas, S., Gustafsson, A.-M., Viklander, P., Marsalek, J., & Viklander, M. (2016). Laboratory study of infiltration into two frozen engineered (sandy) soils recommended for bioretention. *Hydrological Processes*, *30*, 1251–1264. https://doi.org/10.1002/hyp.10711

Motovilov, Y. G. (1978). Mathematical model of water infiltration into frozen soils. *Soviet Hydrology*, *17*(2), 62–66.

Motovilov, Y. G. (1979). Simulation of meltwater losses through infiltration into soil. *Soviet Hydrology*, *18*(3), 217–221.

Painter, S. (2011). Three-phase numerical model of water migration in partially frozen geological media: Model formulation, validation, and applications. *Computational Geosciences*, *15*(1), 69–85.

Pebesma, E. J. (2004). Multivariable geostatistics in S: The gstat package. *Computers & Geosciences*, *30*, 683–691.

Philip, J. R. (1957a). The theory of infiltration: 1. The infiltration equation and its solution. *Soil Science*, *83*(5), 345–358.

Philip, J. R. (1957b). The theory of infiltration: 4. Sorptivity and algebraic infiltration equations. *Soil Science*, *84*(3), 257–264.

Pomeroy, J. W., Gray, D. M., Brown, T., Hedstrom, N. R., Quinton, W. L., Granger, R. J., & Carey, S. K. (2007). The cold regions hydrological model: A platform for basing process representation and model structure on physical evidence. *Hydrological Processes*, *21*, 2650–2667.

Quinton, W. L., Bemrose, R. K., Zhang, Y., & Carey, S. K. (2009). The influence of spatial variability in snowmelt and active layer thaw on hillslope drainage for an alpine tundra hillslope. *Hydrological Processes*, *23*, 2628–2639. https://doi.org/10.1002/hyp.7327

R Core Team (2016). R: A language and environment for statistical computing. R Foundation for Statistical Computing, Vienna, Austria. URL https://www.r-project.org/

Romanovsky, V., & Osterkamp, T. (2000). Effects of unfrozen water on heat and mass transport processes in the active layer and permafrost. *Permafrost and Periglacial Processes*, *11*, 219–239.

Roth, K., Schulin, R., Flühler, H., & Attinger, W. (1990). Calibration of time domain reflectometry for water content measurement using a composite dielectric approach. *Water Resources Research*, *26*, 2267–2273.

Scherler, M., Hauck, C., Hoelzle, M., Stähli, M., & Völksch, I. (2011). Meltwater infiltration into the frozen active layer at an alpine permafrost site. *Permafrost and Periglacial Processes*, *2*(4), 325–334.

Seyfried, M. S., & Murdock, M. D. (1996). Calibration of time domain reflectometry of measurement of liquid water in frozen soils. *Soil Science*, *161*, 87–98.

Spaans, E. J. A., & Baker, J. M. (1995). Examining the use of time domain reflectometry for measuring liquid water content in frozen soil. *Water Resources Research*, *31*, 2917–2925. https://doi.org/10.1029/95WR02769

Stähli, M., Jansson, P.-E., & Lundin, L.-C. (1996). Preferential water flow in a frozen soil—A two-domain model approach. *Hydrological Processes*, *10*, 1305–1316.

Stähli, M., Jansson, P.-E., & Lundin, L.-C. (1999). Soil moisture redistribution and infiltration in frozen sandy soils. *Water Resources Research*, *35*(1), 95–103. https://doi.org/10.1029/1998WR900045.

Su, J. J., van Bochove, E., Thériault, G., Novotna, B., Khaldoune, J., Denault, J. T., … Chow, T. L. (2011). Effects of snowmelt on phosphorus and sediment losses from agricultural watersheds in eastern Canada. *Agricultural Water Management*, *98*(5), 867–876. https://doi.org/10.1016/j.agwat.2010.12.013

Therrien, R., McLaren, R. G., Sudicky, E. A., & Panday, S. M. (2010). *HydroGeoSphere: A three-dimensional numerical model describing fully-integrated subsurface and surface flow and solute transport*. Waterloo, ON: Groundwater Simulations Group, University of Waterloo.

Tindall, J. A., Hemmen, K., & Dowd, J. F. (1992). An improved method for field extraction and laboratory analysis of large, intact soil cores. *Journal of Environmental Quality*, *21*, 259–263.

van der Kamp, G., Hayashi, M., & Gallén, D. (2003). Comparing the hydrology of grassed and cultivated catchments in the semi-arid Canadian prairies. *Hydrological Processes*, *17*(3), 559–575.

Watanabe, K., Kito, T., Dun, S., Wu, J. Q., Greer, R. C., & Flury, M. (2012). Water infiltration into a frozen soil with simultaneous melting of the frozen layer. *Vadose Zone Journal*, *12*(1), 0. https://doi.org/10.2136/vzj2011.0188

Watanabe, K., & Kugisaki, Y. (2017). Effect of macropores on soil freezing and thawing with infiltration. *Hydrological Processes*, *31*(2), 270.

Watanabe, K., & Wake, T. (2009). Measurement of unfrozen water content and relative permittivity of frozen unsaturated soil using NMR and TDR. *Cold Regions Science and Technology*, *59*(1), 34–41. https://doi.org/10.1016/j.coldregions.2009.05.011

Weiler, M., & Flühler, H. (2004). Inferring flow types from dye patterns in macroporous soils. *Geoderma*, *120*, 137–153.

Williams, C. J., McNamara, J. P., & Chandler, D. G. (2009). Controls on the temporal and spatial variability of soil moisture in a mountainous landscape: The signature of snow and complex terrain. *Hydrology and Earth System Sciences*, *13*, 1325–1336.

Zhao, L., & Gray, D. M. (1997). A parametric expression for estimating infiltration into frozen soils. *Hydrological Processes*, *11*, 1761–1775.

Zhao, L., Gray, D. M., & Male, D. (1997). Numerical analysis of simultaneous heat and mass transfer during infiltration into frozen ground. *Journal of Hydrology*, *200*, 345–363.

How to cite this article: Appels WM, Coles AE, McDonnell JJ. Infiltration into frozen soil: From core-scale dynamics to hillslope-scale connectivity. *Hydrological Processes*. 2018;32:66–79. https://doi.org/10.1002/hyp.11399